iScience

Article

Dmcyp12c1 is required for eye development and retinal integrity during aging in *Drosophila*

Graphical abstract

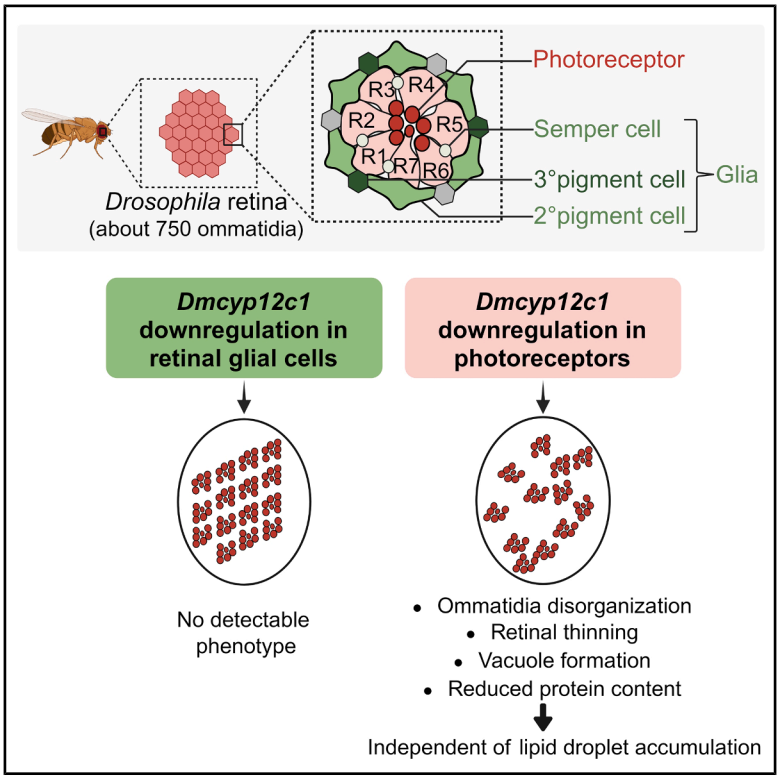

Highlights

- *Dmcyp12c1* gene encodes a retina-enriched CYP450 required for eye development
- Neuronal loss of *Dmcyp12c1* gene drives age-dependent retinal degeneration
- *Dmcyp12c1*-dependent retinal degeneration is independent of lipid dropletaccumulation
- Cholesterol overload does not impair retinal integrity

Authors

Jeanne Serrano, Lucy Martine, Louane Charvet, ..., Niyazi Acar, Elodie A.Y. Masson, Georges Alves

Correspondence

georges.alves@ube.fr

In brief

Lipid; Retinal biology; Cell biology; Aging

Serrano et al., 2026, iScience *29*, 118202
November 20, 2026 © 2026 The Authors. Published by Elsevier Inc.
https://doi.org/10.1016/j.isci.2026.118202

CellPress

iScience

CellPress
OPEN ACCESS

Article

Dmcyp12c1 is required for eye development and retinal integrity during aging in *Drosophila*

Jeanne Serrano,[1,2] Lucy Martine,[2] Louane Charvet,[1] Gérard Manière,[1] Yaël Grosjean,[1] Niyazi Acar,[2,3] Elodie A.Y. Masson,[2] and Georges Alves[1,4,*]

[1]Université Bourgogne Europe, Institut Agro, CNRS, INRAE, UMR CSGA, PERSING Research Group, 21000 Dijon, France
[2]Université Bourgogne Europe, Institut Agro, CNRS, INRAE, UMR CSGA, Eye & Nutrition Research Group, 21000 Dijon, France
[3]Université Bourgogne Europe, CHU Dijon, Public Health Department, Institut Agro, CNRS, INRAE, UMR CSGA, Eye & Nutrition Research Group, 21000 Dijon, France
[4]Lead contact
*Correspondence: georges.alves@ube.fr
https://doi.org/10.1016/j.isci.2026.118202

SUMMARY

Cytochrome P450 (CYP) enzymes regulate lipid metabolism and cellular homeostasis, yet their cell-type specific roles in the retina remain poorly understood. Using *Drosophila melanogaster*, we screened *Cyp* genes predicted to encode homologs of human CYP27A1 and identified *Dmcyp12c1* as highly enriched in the retina and functionally critical in photoreceptors. Developmental photoreceptor-specific downregulation of *Dmcyp12c1* gene reduces eye size and impairs pigmentation, while glial loss produces no phenotype. Adult-specific neuronal downregulation triggers progressive retinal degeneration characterized by ommatidial disorganization, retinal thinning, vacuole formation, and reduced retinal protein content. In contrast, glial downregulation produced no detectable phenotype. Surprisingly, degeneration occurred independently of cholesterol accumulation or lipid droplet formation, and dietary cholesterol supplementation does not reproduce retinal degeneration in control flies. Together, our findings identify the *Dmcyp12c1* gene as a critical regulator of retinal integrity and suggest a mechanism independent of bulk cholesterol accumulation, pointing toward a mitochondrial mechanism underlying CYP-mediated neuroprotection.

INTRODUCTION

Cytochrome P450 (CYP) enzymes constitute an evolutionarily conserved superfamily involved in the metabolism of endogenous and exogenous compounds.[1] CYP enzymes are typically hemoproteins with monooxygenase activity, able to metabolize a broad range of substrates including xenobiotics and endogenous molecules, especially lipids, fatty acids, and sterols.[2,3] Consequently, these enzymes are involved in the metabolism of various compounds and play a crucial role in detoxification and catabolism,[4–6] while also being involved in the production of bioactive molecules.[2,7,8] These signaling molecules play crucial roles, especially in the nervous system, while CYP enzymes are being considered for their involvement in brain development and neurodegenerative diseases.[8–10]

In the mammalian retina, CYP enzymes have been described to hydroxylate cholesterol and contribute to its turnover and elimination in the form of oxysterols.[11] CYP46A1 and CYP27A1 are thought to be the most important ones, and loss of *Cyp46a1* and/or *Cyp27a1* expression has been shown to be associated with retinal sterol accumulation and structural and functional alterations.[12–16] Moreover, modifications of CYP expression and disruptions of sterol homeostasis have been described in a model of degenerative optic neuropathy in rats,[17–19] and a polymorphism in CYP46A1 has also been associated with glaucoma in humans.[20] Importantly, CYP450 enzymes can exhibit cell-specific expression patterns,[21–23] suggesting specialized physiological functions depending on the cellular context. This aspect is particularly relevant in the retina, which relies, as a neuronal tissue, on glia-neuron interactions, to maintain structural and functional integrity. Therefore, identifying the cell-specific role of CYP450 enzymes appears important to better understand the mechanisms underlying maintenance of retinal integrity and development of degenerative diseases.

Drosophila melanogaster is a widely used model organism for investigating the cellular and molecular mechanisms underlying retinal development, function, and degeneration. Its powerful genetic toolkit enables precise, especially cell-type-specific, gene manipulation, making it particularly well suited to dissect the contribution of individual genes and cells to retinal integrity. Like the mammalian retina, the *Drosophila* retina is composed of both neuronal and glial cells. They are organized into approximately 750 ommatidia. Each ommatidium consists of eight neuronal photoreceptor cells and four glial semper cells, all surrounded by a hexagonal arrangement of nine glial retinal pigment cells (RPCs), including six secondary and three tertiary RPCs (Figure 1).[24,25] The CYP superfamily has been extensively characterized in *Drosophila melanogaster*, with approximately 90

This is an open access article under the CC BY license (http://creativecommons.org/licenses/by/4.0/).

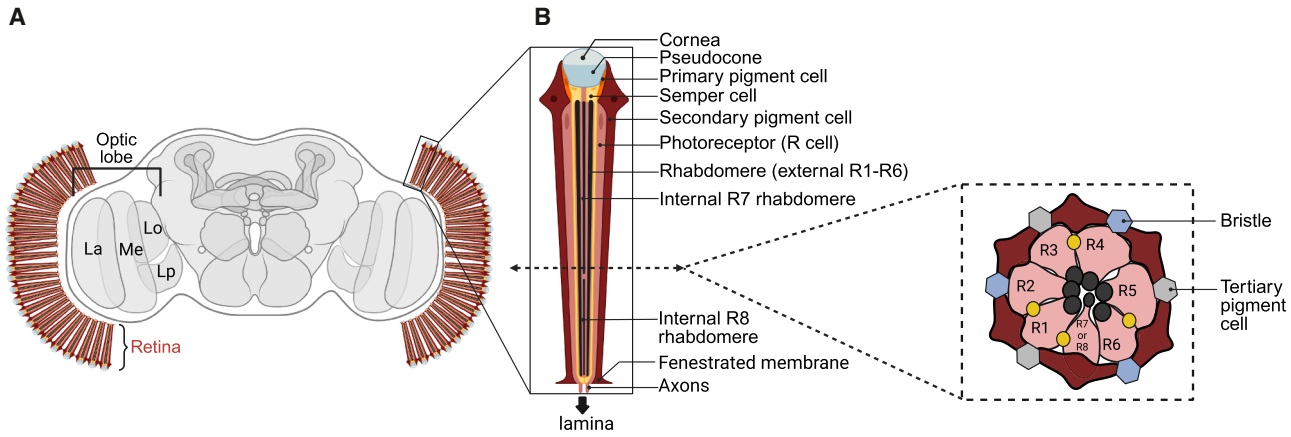

Figure 1. Structural organization of the adult *Drosophila* retina

(A) Schematic representation of a longitudinal section of *Drosophila* brain and retina. The optic lobes consist of the lamina (La), medulla (Me), lobula (Lo), and lobula plate (Lp). The retina is composed of approximately 750 ommatidia.

(B) Schematic representation of a longitudinal section of an ommatidium. A scheme of a cross-section of an ommatidium is shown in the box. Created with BioRender.com.

CYP genes annotated in the genome and identified roles in detoxification and hormone biosynthesis.[26–29] However, while lipid accumulation seems to be a driver of photoreceptor degeneration,[30,31] the potential contribution of CYP enzymes to retinal physiology and integrity maintenance in flies remains largely unexplored.

In the present study, we use *Drosophila melanogaster* as a genetic model to investigate the potential cell-specific role of CYP enzymes, focusing on CYP27A1, in the maintenance of retinal integrity and glia-neuron interactions. Among the eight human candidate CYP27A1-related CYPs with unknown function, we showed that *Dmcyp12c1*, *Dmcyp12a5*, and *Dmcyp49a1* genes are highly expressed in the *Drosophila* retina. Interestingly, the developmental downregulation of *Dmcyp12c1* gene specifically in photoreceptors resulted in decreased eye size at emergence. Moreover, the neuronal *Dmcyp12c1* gene appears to play a crucial role in maintaining retinal integrity during aging. Indeed, its downregulation in photoreceptors, but not in glial cells, induced ommatidial disorganization and retinal thinning together with the appearance of vacuoles characteristic of retinal degeneration, without detectable lipid accumulation. Our findings reveal a neuron-specific role for *Dmcyp12c1* gene and uncover a mechanism of retinal degeneration that is independent of cholesterol accumulation.

RESULTS

Dmcyp12c1 gene encodes a retina-enriched CYP450 required for eye development

We first identified eight candidate *Drosophila* CYPs with predicted homology to human CYP27A1: DmCYP12A4, DmCYP12A5, DmCYP12B2, DmCYP12C1, DmCYP12D1, DmCYP12E1, DmCYP49A1, and DmCYP301A1, whose function remains unknown so far. The percentage of amino acid identity with the CYP27A1 protein ranged from 24% to 28%, while the percentage of similarity ranged from 42% to 49% (Table S2). The selected *Drosophila* CYP genes were previously identified as encoding mitochondrial proteins, consistent with the human CYP27A1 protein.

We determined which cyp genes were expressed in the *Drosophila* retina by performing quantitative PCR analyses to compare transcript levels in the heads of eyeless flies carrying the *GMR-hid* transgene with control flies. We detected a strong decrease in the transcript levels of *Dmcyp12a5* (−18.8%), *Dmcyp12c1* (−39%), and *Dmcyp49a1* (−47.4%) in eyeless fly heads compared with control fly heads. This result indicates that *Dmcyp12a5*, *Dmcyp12c1*, and *Dmcyp49a1* are highly expressed in the retina compared with the whole head. Transcript levels of *Dmcyp12a4*, *Dmcyp12b2*, *Dmcyp12d1*, *Dmcyp12e1*, and *Dmcyp301a1* genes did not show a reduced expression in the head of eyeless flies, indicating their absence or their relatively low expression in the retina (Figure 2A). On the contrary, to determine a potential role of *Dmcyp12a5*, *Dmcyp12c1*, and *Dmcyp49a1* genes in eye development, we used dsRNA under the control of the *GMR-Gal4* driver to specifically downregulate the expression of these 3 genes in the eye (see genetic tools in Figure S1). We observed a significantly decreased expression of *Dmcyp12a5* and *Dmcyp12c1* genes in the entire head following retinal-specific downregulation, whereas *Dmcyp49a1* gene expression was not significantly affected. These results support the specificity and efficiency of the dsRNA constructs and the high expression of these *Dmcyp12c1* and *Dmcyp12a5* genes in the retina compared with Dmcyp49a1 gene (Figure 2B).

We then studied the role of *Dmcyp12c1* and *Dmcyp12a5* genes in retinal development by specifically downregulating their eye expression. The downregulation of *Dmcyp12c1* gene expression using the pan-retinal *GMR-Gal4* driver resulted in a 43% reduction of the eye size compared with the control flies (Figures 2C and 2D). Downregulation of *Dmcyp12a5* gene during development did not result in eye defect (data not shown). To investigate the implication of the different retinal cell types, we specifically downregulated the gene expression in either retinal

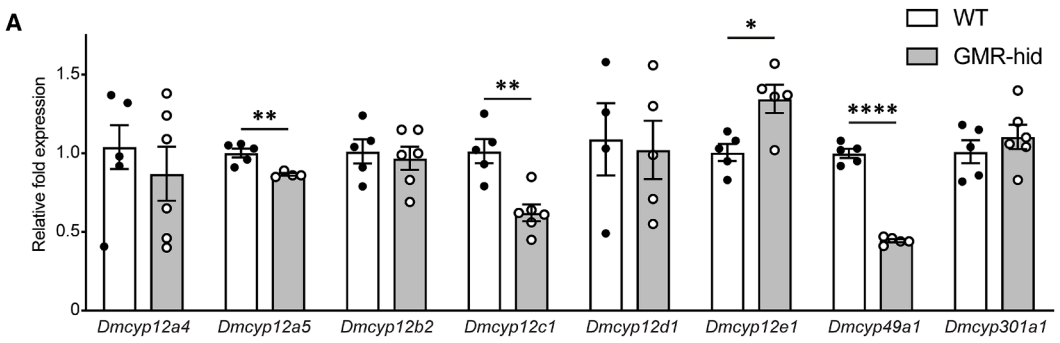

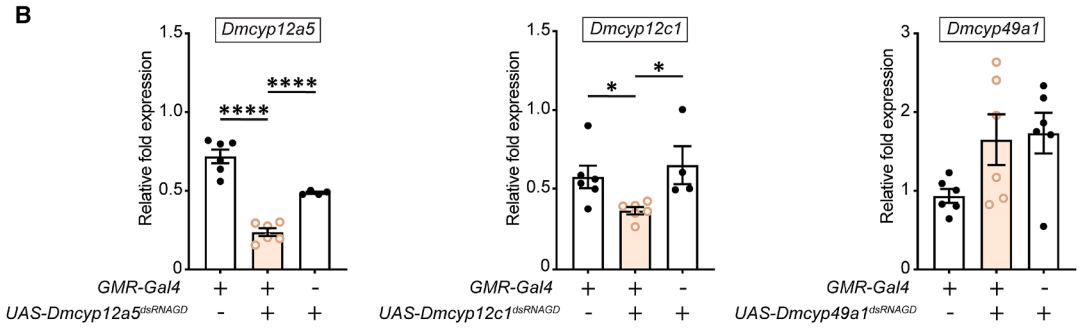

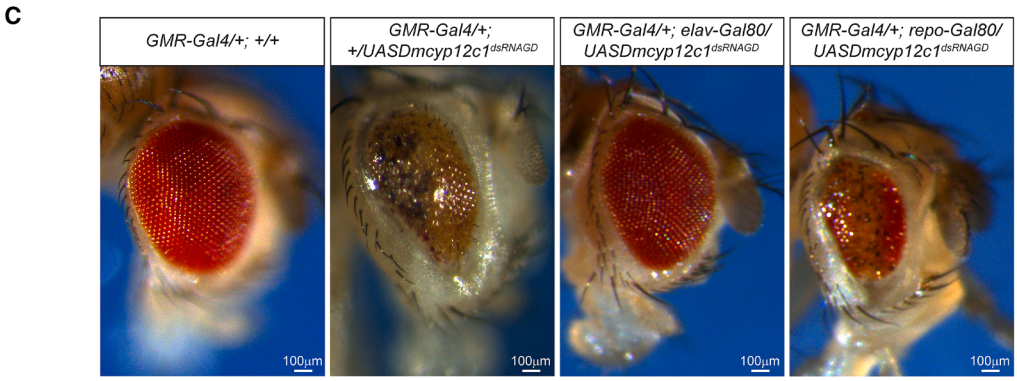

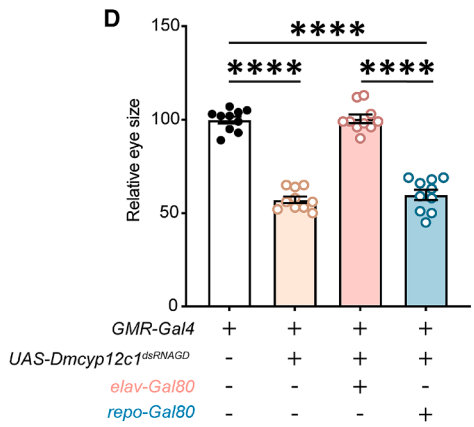

(legend on next page)

glial cells using the *elav-Gal80* driver or neuronal retinal cells using the *repo-Gal80* driver (see genetic tools in Figures S1A and S1B). Whereas downregulation of *Dmcyp12c1* gene in glial cells did not modify the eye size, a 40% reduction compared with controls was observed after it was downregulated in photoreceptors (Figures 2C and 2D). This reduction of eye size was accompanied by a loss of eye pigmentation, indicating a rough eye phenotype. Consequently, the expression of *Dmcyp12c1* gene in retinal neurons appears to be required for the proper development of the *Drosophila* eye.

Neuronal loss of *Dmcyp12c1* gene drives age-dependent retinal degeneration

Since *Dmcyp12c1* gene is required for eye development and highly expressed in the retina, we decided to investigate the effects of *Dmcyp12c1* gene downregulation during adulthood. To study the effects of specific adult downregulation of *Dmcyp12c1* gene, we added the tubulin-Gal80ts transgene to the previous genetic combination to block dsRNA expression during development (see Figure S1C for a schematic description of the genetic tools). We then verified that *Dmcyp12c1* gene is expressed during adulthood. Relative transcript levels after *Dmcyp12c1* dsRNA expression in the retina showed a trend toward reduction in both glial cells and photoreceptors 7 days post-emergence, which was confirmed at 30 days, indicating that *Dmcyp12c1* gene is also highly expressed in both cell types in adults (Figure 3A).

We further investigated the importance of *Dmcyp12c1* gene in the *Drosophila* eye by determining whether it is also required in the retina during adulthood. The downregulation of *Dmcyp12c1* gene in the retinal glial cells at adulthood did not result in any observable defect. Indeed, the ommatidia layout and retinal sections at 7 and 30 days post-emergence appeared similar to the controls (Figures 3B, 3C, and 3E). Interestingly, the downregulation of *Dmcyp12c1* gene in photoreceptors induced a significant disorganization of the ommatidia observable at 30 days but not as early as 7 days. Indeed, ommatidia were not properly spaced and the equator line that defines the retinal polarity was not apparent (Figure 3B). Interestingly, we also observed a 40% reduction in retinal thickness on *Drosophila* head cryosections (Figures 3C and 3D). Moreover, using toluidine blue coloration on semi-thin retina sections, we highlighted the presence of vacuoles (Figure 3E). Notably, pigment distribution was not homogeneous and pigment aggregates were observed, suggesting a loss of pigmentary cells, these cells being responsible for the shape and precise arrangement of the ommatidia. To get better insight into these modifications, we examined the levels of retinal proteins. Consistent with the degenerative phenotype described above, we noticed a 38% decrease in the retinal protein levels of aged flies with *Dmcyp12c1* gene downregulation specifically in retinal photoreceptors compared with controls, thus reflecting retinal cell death (Figure 3F). Altogether, these results indicate that the downregulation of *Dmcyp12c1* gene in photoreceptors, but not in glial cells, leads to progressive retinal degeneration during aging, ultimately impacting all retinal cell types.

Dmcyp12c1-dependent retinal degeneration is independent of cholesterol accumulation

Given the known involvement of CYP enzymes in lipid metabolism in mammals, we next investigated whether the retinal degeneration alters retinal lipid composition. We did not notice a significant change in retinal cholesterol levels per retina after *Dmcyp12c1* gene downregulation in either glial cells or photoreceptors, although there was an upward trend at 30 days (Figure 4A). We also examined lipid droplets, which serve as lipid storage deposits, particularly for excess cellular cholesterol, using cryosections of *Drosophila* heads. We found no evidence of cholesterol accumulation in retinal lipid droplets compared with the fat body adjacent to the retina, which is highly enriched in lipids. This was confirmed using Nile red and LipidTOX stainings, two general markers of neutral lipids such as triglycerides and cholesteryl esters, which are lipid species typically stored in intracellular lipid droplets (Figures 4B and 4C). Overall, our observations indicate that photoreceptor-specific *Dmcyp12c1* downregulation disrupts retinal architecture independently of local cholesterol and lipid droplet accumulation.

Cholesterol supplementation does not impair retinal integrity

To further test the role of cholesterol, we reared the flies on a cholesterol-enriched diet. After 7 days of exposition, the cholesterol was effectively incorporated into the retina as shown by the 27-fold increase in retinal cholesterol levels in young flies (Figure 5A) compared with those raised on a standard diet (Figure 4A). Although fly lines carrying the *GMR-Gal4* transgene exhibited higher protein levels in aged flies compared to those lacking this transgene, retinal cholesterol levels were similar (Figure 5A). Moreover, despite the fact that the cholesterol-enriched diet induced a substantial increase in retinal cholesterol, it was not associated with any structural retinal defects (Figures 5B and 5C). These findings indicate that cholesterol accumulation following rearing on a cholesterol-supplemented diet does not adversely affect *Drosophila* retinal morphology.

Figure 2. *Dmcyp12c1* is a retina-enriched CYP that is essential in neurons for proper eye development

(A) Relative expression of the *Dmcyp450* gene in the head of control and eyeless flies (GMR-hid) flies. All quantitative reverse-transcription PCR (RT-qPCR) experiments were performed on 7-day-old *Drosophila*. All data are presented as mean ± SEM of 4-6 biological replicates represented by circles. $*p < 0.05$, $**p < 0.01$,$***p < 0.001$ (unpaired two-tailed t-tests).

(B) Relative expression of *Dmcyp450* genes in *Drosophila* heads after retinal downregulation. Specific retinal expression of the $Dmcyp12a5^{dsRNAGD}$, $Dmcyp12c1^{dsRNAGD}$, and $Dmcyp49a1^{dsRNAKK}$ was under the control of GMR-Gal4 driver. All RT-qPCR experiments were performed on 7-day-old *Drosophila*. All RT-qPCR data are presented as mean ± SEM of 4–6 biological replicates represented by circles. $*p < 0.05$, $**p < 0.01$, $****p < 0.0001$ (unpaired two-tailed *t* tests).

(C) Light micrographs, in order, of the eyes of 3-day-old control flies and flies after downregulation of *Dmcyp12c1* gene in all retinal cell types, in retinal glial cells or in photoreceptors. Scale bars represent 100 μm.

(D) Relative eye size of each experimental group compared with the control line (*GMR-Gal4*/+). Data are presented as mean ± SEM of 10 biological replicates represented by circles. $****p < 0.0001$ (ordinary one-way ANOVA followed by Tukey's multiple comparisons test).

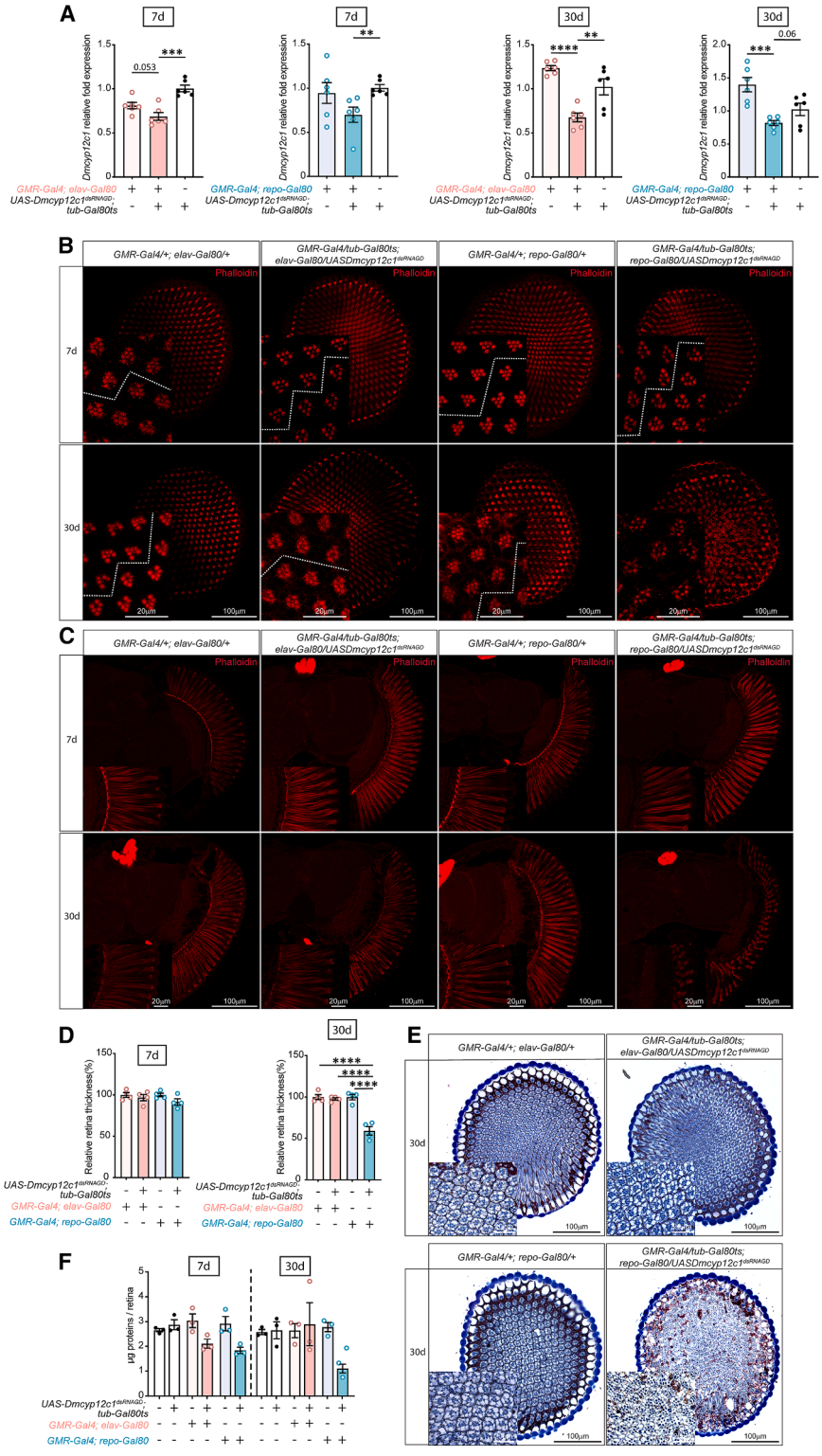

Figure 3. Neuronal *Dmcyp12c1* expression maintains retinal integrity during aging

(A) *Dmcyp12c1* transcript levels in *Drosophila* head after its downregulation in the retina. *Dmcyp12c1* gene was downregulated after fly emergence (using *UAS-Dmcyp12c1*^{dsRNAGD}) either in glial cells (using *GMR-Gal4; elav-Gal80*) or in photoreceptors (using *GMR-Gal4; repo-Gal80*). All RT-qPCR experiments were performed on the heads of *Drosophila* that were 7–12 days old or 30–35 days old. All data are presented as mean ± SEM of 6 biological replicates represented by circles. $^{**}p < 0.01$, $^{***}p < 0.001$, $^{****}p < 0.0001$ (unpaired two-tailed *t* tests).

(B) *Dmcyp12c1* gene was downregulated post-emergence (using *UAS-Dmcyp12c1*^{dsRNAGD}*; tub-Gal80ts*) either in glial cells or in photoreceptors. All analyses were done on dissected retinas of young flies (7–10 days old) or aged flies (30–35 days old) reared on standard food. Retinal neurons, rich in F-actin, were visualized in whole-mounted retinas with phalloidin, an actin filament-specific probe, using a confocal microscope. Scale bars represent 100 µm at low magnification (×40) and 20 µm at high magnification (box, ×63). The dotted white line defines the equator of the retina, which is the symmetry between the dorsal and ventral parts.

(C and D) Photoreceptors were also visualized with phalloidin on head cryosections of 7- to 12-day-old or 30- to 35-day-old *Drosophila* after downregulation of *Dmcyp12c1* gene expression in retinal glial cells or in photoreceptors (C) and retina thickness was measured (D). (C) Scale bars represent 100 µm at low magnification (x20) and 20 µm at high magnification (box, x100). (D) Data are expressed relative to respective control and presented as mean ± SEM of 4 biological replicates represented by circles. $^{****}p < 0.0001$ (ordinary one-way ANOVA followed by Tukey's multiple comparisons).

(E) Coloration with toluidine blue of semi-thin sagittal sections of half heads of 30- to 35-day-old control flies or flies with *Dmcyp12c1* down-regulation in glial cells or in retinal photoreceptors. Scale bars represent 100 µm at low magnification (×20) and 20 µm at high magnification (box, ×100). 3–4 biological replicates per condition were used.

(F) Protein levels per retina. Data are presented as mean ± SEM of 3 biological replicates individually represented by circles. Each biological replicate was composed of a pool of 150 retinas.

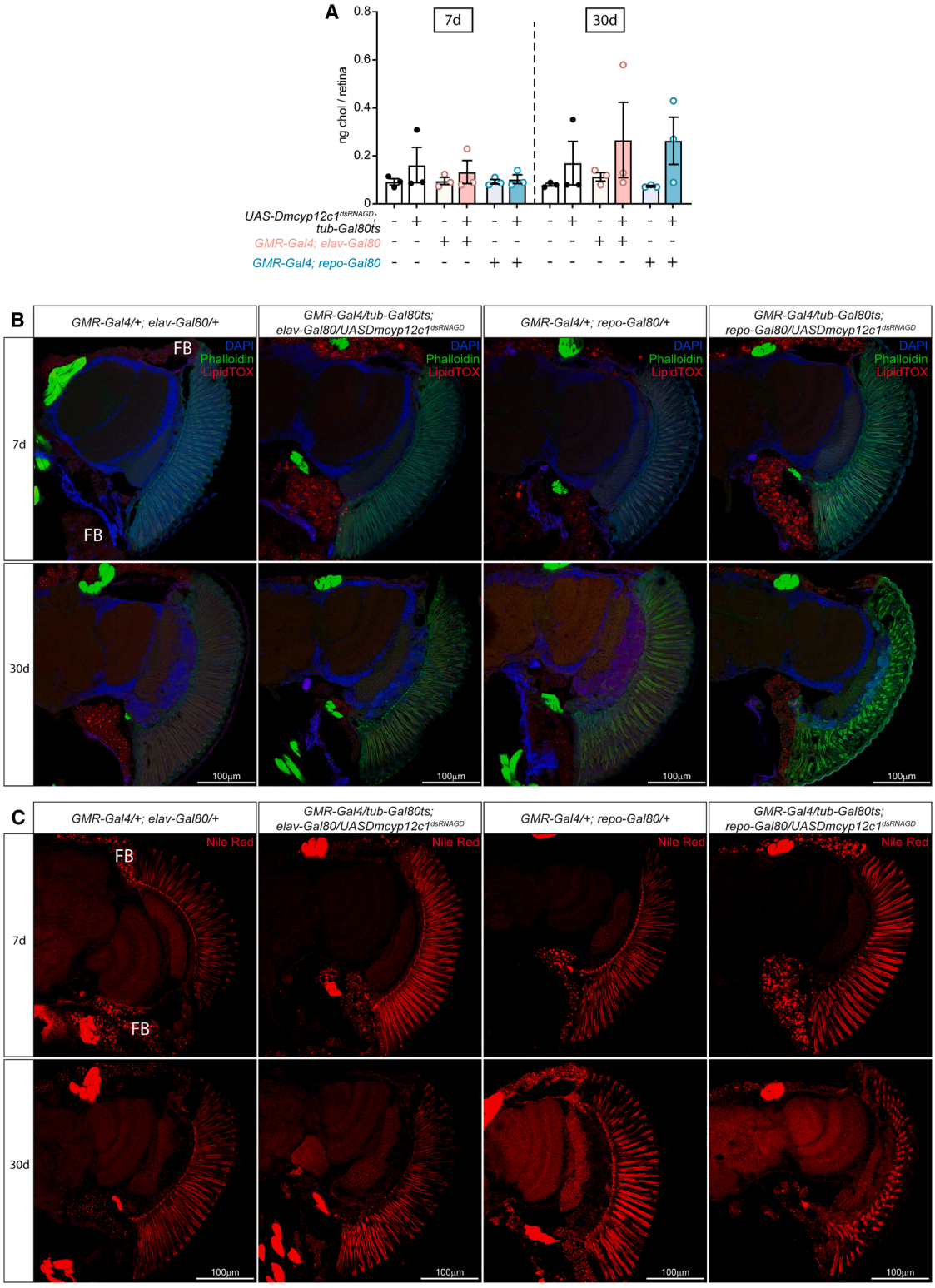

Figure 4. *Dmcyp12c1*-dependent retinal degeneration is not associated with lipid accumulation

Dmcyp12c1 was downregulated post-emergence (using *UAS-Dmcyp12c1^{dsRNAGD}; tub-Gal80ts*) either in glial cells (using *GMR-Gal4*; *elav-Gal80*) or in photoreceptors (using *GMR-Gal4; repo-Gal80*). All analyses were done on dissected retinas of young flies (7–10 days old) or aged flies (30–35 days old) reared on standard food. For each graph, the first four bars represent the values for the control genotypes.

(legend continued on next page)

DISCUSSION

CYP enzymes are widely recognized for their roles in metabolizing endogenous compounds such as cholesterol, fatty acids, hormones, vitamins, and neuromediators, as well as in detoxifying xenobiotics, all these processes being critical for neuronal homeostasis.[8–10,32] However, their contribution to retinal physiology and degeneration remains poorly understood. In this study, we identified *Dmcyp12c1* gene as a critical, cell-type-specific regulator of retinal development and age-dependent retinal integrity in *Drosophila melanogaster*. Our data demonstrate that DmCYP12C1 function is intrinsically required in photoreceptors, both during development and adulthood in order to preserve retinal architecture. Developmental downregulation leads to reduced eye size and pigmentation defects, while adult-specific neuronal downregulation induces progressive retinal degeneration characterized by ommatidial disorganization, vacuolization, and retinal thinning. Importantly, glial-specific downregulation does not recapitulate these phenotypes. This finding is particularly notable given the well-established metabolic coupling between neurons and glia in the retina.[33–35] It suggests that DmCYP12C1 performs a cell-autonomous function in photoreceptors that is essential for maintaining retinal architecture, while its loss secondarily impacts the surrounding glial cells, as reflected by pigment disorganization and altered retinal structure.

DmCYP12C1 was selected based on predicted homology to human CYP27A1, which has been reported to contribute to retinal integrity in rodents.[12,13] CYP27A1 is a mitochondrial cholesterol hydroxylase involved in cholesterol efflux, and its loss in rodents leads to structural retinal defects, especially in retinal vessels, associated with cholesterol and other sterol accumulation in the retina.[12] Moreover, cholesterol and lipid droplet accumulation have already been observed in association with retinal degeneration in the fly.[30,31,36] Therefore, we looked for evidence of altered sterol homeostasis in our *Drosophila* model with *Dmcyp12c1* gene downregulation. Our results showed no changes in retinal cholesterol levels or lipid droplet content following *Dmcyp12c1* gene downregulation. Moreover, dietary cholesterol supplementation did not reproduce the degenerative phenotype despite markedly increased retinal cholesterol levels. Altogether, these observations support the idea that bulk cholesterol accumulation or gross lipid droplet expansion are unlikely to be the primary drivers of retinal degeneration in this model. However, they do not rule out the potential contribution of localized lipid changes, e.g., within photoreceptors or within membranes, or undetected alterations in specific sterol species. Indeed, cholesterol represents only a minor fraction of the total sterols in *Drosophila* (less than 3% in the head),[37] raising the possibility that the levels of other sterols, such as dietary phytosterols (e.g., sitosterol, campesterol, or stigmasterol), which may serve as substrates for CYP enzymes, are altered upon DmCYP12C1 loss. Such changes would not necessarily be detected by bulk cholesterol measurements and may also be incompletely captured by lipid droplet staining approaches, which primarily report on neutral lipid storage.

Beside contributing to cholesterol elimination and avoiding its accumulation, oxysterol production by CYP enzymes can have direct effects on retinal cell metabolism. Indeed, oxysterols are signaling molecules that are ligands for nuclear receptors. They have also been described as allosteric modulators of neurotransmitter receptors and to play a role in neuron survival, as is the case for CYP46A1 and its product 24S-hydroxycholesterol in mammals.[10] CYP enzymes also produce other signaling molecules from polyunsaturated fatty acids that are oxylipins (epoxy-PUFAs and hydroxy-PUFAs), with potential implications in neuroprotection by resolution of inflammation and oxidative stress.[8] Loss of CYP activity could thus be deleterious for the retina by being at the origin of a lack of lipid mediators.

Interestingly, our study further reveals that *Drosophila* retina tolerates substantial increases in cholesterol without structural disruption, in contrast to mammalian systems where cholesterol accumulation is often deleterious.[38–40] This divergence underscores species-specific differences in sterol metabolism and suggests that cholesterol-independent mechanisms may play a more prominent role in fly retinal degeneration. In our study, a cholesterol-supplemented diet induces a robust increase in retinal cholesterol but is not associated to any structural defects. In previous reports, high cholesterol levels can extend lifespan, particularly on moderate-to high-protein diets.[41] In contrast, Phillips et al. (2008) reported in a *Drosophila* model of Niemann-Pick type C disease that impaired cholesterol trafficking leads to cholesterol accumulation in neurons and the retina, which correlates with progressive neurodegeneration, including reduced photoreceptor function and retinal disorganization.[30] This suggests that the effects of cholesterol overload may vary depending on its localization, the genetic background, and the overload level.

Beyond its predicted relationship to CYP27A1, DmCYP12C1 belongs to the *Drosophila* CYP12 family, which together with the CYP49, CYP301, CYP302, CYP314, and CYP315 families forms the fly mitochondrial (MITO) clan of CYP enzymes.[29] Orthology analyses place the human mitochondrial CYP27 subfamily members, CYP27A1, CYP27B1, and CYP27C1, together with CYP24A1, among the closest vertebrate relatives of the insect CYP12 proteins. Interestingly, the founding member of the subfamily, CYP12B1, was originally reported to be most closely related to the vitamin D3-metabolizing CYP24 family.[42] This phylogenetic grouping reflects a shared ancestry among class I, ferredoxin/ferredoxin-reductase-dependent P450 enzymes anchored in the inner mitochondrial membrane, rather than strict functional equivalence between fly and vertebrate proteins.[43,44] Because of the diverse substrate specificities of vertebrate

(A) Cholesterol levels per retina. Data are presented as mean ± SEM of 3 biological replicates individually represented by circles. Each biological replicate was composed of a pool of 150 retinas.

(B) Cryosections of *Drosophila* heads stained with phalloidin to visualize F-actin (green), which is highly abundant in photoreceptors, and with LipidTOX to visualize lipid droplets. Scale bars represent 100 μm (×20). 3–4 biological replicates per condition were used.

(C) Cryosections of *Drosophila* heads stained with Nile red to label neutral lipids localized both in lipid droplets (red) and in rhabdomeres. Scale bars represent 100 μm (×20). 3–4 biological replicates per condition were performed. FB, fat body.

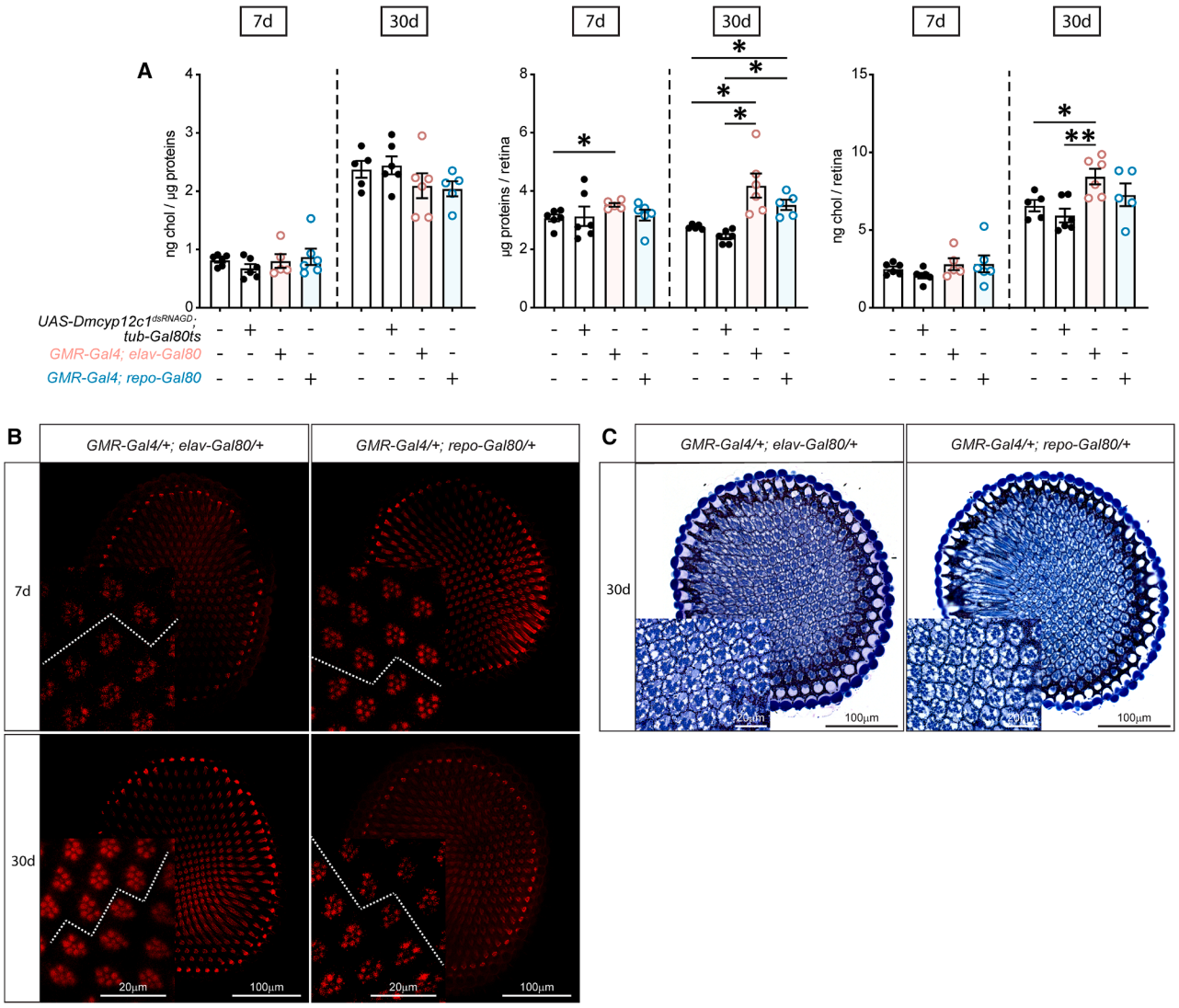

Figure 5. Cholesterol overload does not impair retinal structure in *Drosophila*

Control flies were studied. All measures were done on dissected retinas of young flies (7–10 days old) or aged flies (30–35 days old) reared on cholesterol-supplemented food.

(A) Protein levels per retina (left) and cholesterol levels per retina (right). Data are presented as mean ± SEM of 4–6 biological replicates individually represented by circles. Each biological replicate was made of a pool of 30 retinas. $^{*}p < 0.05$, $^{**}p < 0.01$ (ordinary one-way ANOVA followed by Tukey's multiple comparisons).

(B) Photoreceptor staining 7 or 30 days after post-emergence in control flies. Retinal neurons, rich in F-actin, were visualized in whole-mounted retinas with phalloidin, an actin filament-specific probe, using a confocal microscope. Scale bars represent 100 µm at low magnification (×40) and 20 µm at high magnification (box, ×63). The dotted white line defines the equator of the retina, the symmetry between the dorsal and ventral parts.

(C) Coloration with toluidine blue of semi-thin sagittal sections of half heads of 30- to 35-day-old control flies. Scale bars represent 100 µm at low magnification (×20) and 20 µm at high magnification (box, ×100). 3–4 biological replicates per condition were used.

CYP24A1 and CYP27B1 enzymes, which metabolize vitamin D_3 derivatives and sterols, and the ability of CYP27C1 to catalyze retinoid desaturation,[43–45] this evolutionary relationship raises the possibility that DmCYP12C1 acts on specific lipophilic substrates in photoreceptors, such as ecdysteroid precursors, oxysterols, or retinoid-like compounds, rather than directly regulating bulk cholesterol levels. Substrates of this kind would be consistent with the absence of a bulk cholesterol phenotype in our model while still accounting for a retina-specific requirement for DmCYP12C1, and they offer a testable framework for future metabolomic identification of its endogenous substrate(s).

One possible role is that DmCYP12C1 participates in the mitochondrial metabolic regulation and redox homeostasis. Members of the CYP12 family are localized in mitochondria, where they can influence lipid oxidation, sterol metabolism, and reactive oxygen species (ROS) production.[45,46] Dysregulation of mitochondrial ROS is a well-established driver of age-related retinal degeneration.[47,48] In this context, the previous reported

upregulation of *Dmcyp12c1* gene under oxidative stress conditions (e.g., hyperoxia and paraquat exposure) is particularly informative, as it suggests that DmCYP12C1 may act as part of a protective stress-response pathway.[49] We therefore propose that loss of DmCYP12C1 in photoreceptors leads to increased oxidative stress and mitochondrial dysfunction, which could propagate to neighboring cells and disrupt overall retinal homeostasis Although this hypothesis remains to be directly tested, it provides a mechanistic framework that is consistent with both, our observations and the broader literature on mitochondrial contributions to neurodegeneration.[50–52]

Our findings also highlight an important conceptual distinction between primary neuronal defects and secondary tissue remodeling. While degeneration is initiated in photoreceptors, the observed alterations in pigment cell organization and retinal structure indicates that intercellular signaling between neurons and glia is compromised. This is consistent with emerging evidence that neuronal metabolic stress can induce glial dysfunction, thereby amplifying degenerative processes. In this regard DmCYP12C1 may represent a key molecular link between intracellular metabolic regulation and intercellular communication within the retina.

In conclusion, our study identifies DmCYP12C1 as a previously uncharacterized regulator of retinal integrity with a primary neuron-specific requirement that secondarily impacts surrounding glial cells. We show that retinal degeneration induced by its loss occurs independently of lipid accumulation, pointing instead toward a role of mitochondrial or redox homeostasis. These findings not only expand our understanding of CYP functions in the nervous system but also establish a framework for investigating how mitochondrial metabolic enzymes contribute to neurodegeneration and neuron-glia interactions during aging.

Limitations of the study

Our findings support an essential role for DmCYP12C1 in maintaining retinal integrity, but several limitations of the present study and important questions remain to be addressed. First, we used a single *Dmcyp12c1*^{dsRNA} line, raising the possibility of off-target effects. To assess this possibility, we used the UP-TORR database and identified *Dmcyp12a5* as a potential off-target gene of the *Dmcyp12c1* ^{dsRNA} line, based on a shared 21-bp sequence. In our study, we tested the effect of *Dmcyp12a5* downregulation during retinal development and found no detectable retinal defects. These findings support the conclusion that the retinal phenotype observed is more likely to result from Dmcyp12c1 downregulation than from off-target effects involving other *Dmcyp12* family members. Second, our experiments give indirect information about the expression pattern of *Dmcyp12c1* gene in the eye. Reduced expression in eyeless flies strongly suggests that *Dmcyp12c1* gene is highly expressed in the retina. Furthermore, we used the genetic GMR-Gal4/elav-Gal80 and GMR-Gal4/repo-Gal80 combinations to invalidate cell specifically *Dmcyp12c1* gene expression in the retina in either glial cells or photoreceptors. The expression domains generated by the GMR-Gal4/elav-Gal80 and GMR-Gal4/repo-Gal80 combinations to target glial and neuronal cell types, respectively, were chosen based on previously described expression patterns.[53–55] Indeed, elav-Gal80 and repo-Gal80 have previously been used to suppress GAL4 activity in either neurons or glial cells in the eye.[31] Using UAS-nlsGFP reporter gene, we have confirmed that GMR-Gal4/elav-Gal80 and GMR-Gal4/repo-Gal80 combinations drive specific expression in retinal glial cells and neurons, respectively, in adult eyes (data not shown). Therefore, the degeneration phenotype observed with specific downregulated expression in photoreceptors indirectly showed that *Dmcyp12c1* is expressed in these cells during development and aging. However, direct approaches such as *in situ* hybridization, reporter-based expression analysis, or cell-specific transcript profiling will be required to precisely define its expression pattern within the retina. Moreover, the precise cellular localization of DmCYP12C1 in the retina remains to be determined to confirm its mitochondrial localization. The future study of its expression pattern would provide further insights into its role in neuron-glia interactions and retinal homeostasis. Third, the endogenous substrate(s) and product(s) of DmCYP12C1 in the retina remain unknown. Identifying these substrates and products through targeted or untargeted metabolomic approaches will be essential to define the biochemical pathway(s) involved. Fourth, direct measurements of mitochondrial function, ROS levels, and apoptotic markers will be necessary to define the proposed link between DmCYP12C1 and oxidative stress. Finally, genetic rescue experiments including the use of catalytically inactive mutants will help determine whether DmCYP12C1 enzymatic activity per se is required or whether the protein also fulfills structural or signaling roles. Addressing these questions would provide insights into the molecular mechanisms by which DmCYP12C1 maintains retinal integrity and also a broader knowledge of the contribution of mitochondrial CYP enzymes to neuronal health and age-related neurodegeneration.

RESOURCE AVAILABILITY

Lead contact

Requests for further information and resources should be directed to and will be fulfilled by the lead contact, Dr. Georges Alves (georges.alves@u-bourgogne.fr).

Materials availability

This study did not generate new unique reagents.

Data and code availability

All data reported in this paper will be shared by the lead contact upon request. This paper does not report original code. Any additional information required to reanalyze the data reported in this paper is available from the lead contact upon request.

ACKNOWLEDGMENTS

We are grateful to Serge Loquin and Amandine Chlémaire for their technical support. We also thank the DImaCELL platform for granting access to the confocal microscope. Finally, we would like to thank Amandine Bataille and Elisabeth Dubus from the Imaflow platform for conducting all the preparations for toluidine blue staining experiments. We would like to express our gratitude to the Université Bourgogne Europe, the INRAE, the CNRS, and the Conseil régional de Bourgogne-Franche-Comté for their financial support. This research was additionally supported by the Conseil régional de Bourgogne-Franche-Comté (to Y.G. and N.A.) and the ANR (ANR Pepneuron grant ANR-21-CE16-0027 to Y.G.).

AUTHOR CONTRIBUTIONS

Conceptualization, J.S., E.A.Y.M., and G.A.; validation, J.S., E.A.Y.M., and G.A.; formal analysis, J.S, E.A.Y.M., and G.A.; investigation, J.S., L.M., L.C., G.M., E.A.Y.M., and G.A.; writing – original draft, J.S., E.A;Y.M., and G.A.; writing – review and editing, J.S., L.M. G.M., Y.G., N.A., E.A.Y.M., and G.A.; visualization, J.S.; supervision, E.A.Y.M. and G.A.; funding acquisition, E.A.Y.M., N.A., and Y.G.

DECLARATION OF INTERESTS

The authors declare no competing interests.

DECLARATION OF GENERATIVE AI AND AI-ASSISTED TECHNOLOGIES IN THE MANUSCRIPT PREPARATION PROCESS

Claude (Anthropic) was used on a limited basis to assist with the wording of a few sentences and improve language clarity. The authors reviewed and edited the content generated with the assistance of this tool and take full responsibility for the content of the manuscript.

STAR★METHODS

Detailed methods are provided in the online version of this paper and include the following:

- KEY RESOURCES TABLE
- EXPERIMENTAL MODEL AND STUDY PARTICIPANT DETAILS
  - Fly stocks and rearing conditions
- METHOD DETAILS
  - Selection of *Drosophila* Dmcyp gene
  - Gene expression analysis by real time qPCR
  - Cholesterol quantification by gas chromatography coupled to mass spectrometry (GC-MS)
  - Quantitative determination of protein contents
  - Whole eye imaging
  - Immunohistochemistry
  - Toluidine blue staining
- QUANTIFICATION AND STATISTICAL ANALYSIS
  - Retinal thickness measurement
  - Statistical analysis

SUPPLEMENTAL INFORMATION

Supplemental information can be found online at https://doi.org/10.1016/j.isci.2026.118202.

Received: June 12, 2026
Revised: September 11, 2026
Accepted: October 27, 2026

REFERENCES

1. Sezutsu, H., Le Goff, G., and Feyereisen, R. (2013). Origins of P450 diversity. Philos. Trans. R. Soc. B *368*, 20120428. https://doi.org/10.1098/rstb.2012.0428.
2. Hossam Abdelmonem, B., Abdelaal, N.M., Anwer, E.K.E., Rashwan, A.A., Hussein, M.A., Ahmed, Y.F., Khashana, R., Hanna, M.M., and Abdelnaser, A. (2024). Decoding the Role of CYP450 Enzymes in Metabolism and Disease: A Comprehensive Review. Biomedicines *12*, 1467. https://doi.org/10.3390/biomedicines12071467.
3. McDonnell, A.M., and Dang, C.H. (2013). Basic Review of the Cytochrome P450 System. J. Adv. Pract. Oncol. *4*, 263–268. https://doi.org/10.6004/jadpro.2013.4.4.7.
4. Coelho, A., Fraichard, S., Le Goff, G., Faure, P., Artur, Y., Ferveur, J.F., and Heydel, J.M. (2015). Cytochrome P450-Dependent Metabolism of Caffeine in Drosophila melanogaster. Zhu KY. PLoS One *10*, e0117328. https://doi.org/10.1371/journal.pone.0117328.
5. Esteves, F., Rueff, J., and Kranendonk, M. (2021). The Central Role of Cytochrome P450 in Xenobiotic Metabolism—A Brief Review on a Fascinating Enzyme Family. J. Xenobiot. *11*, 94–114. https://doi.org/10.3390/jox11030007.
6. Lu, K., Song, Y., and Zeng, R. (2021). The role of cytochrome P450-mediated detoxification in insect adaptation to xenobiotics. Curr. Opin. Insect Sci. *43*, 103–107. https://doi.org/10.1016/j.cois.2020.11.004.
7. Pikuleva, I.A. (2006). Cholesterol-metabolizing cytochromes P450. Drug Metab. Dispos. *34*, 513–520. https://doi.org/10.1124/dmd.105.008789.
8. Sarparast, M., Dattmore, D., Alan, J., and Lee, K.S.S. (2020). Cytochrome P450 Metabolism of Polyunsaturated Fatty Acids and Neurodegeneration. Nutrients *12*, 3523. https://doi.org/10.3390/nu12113523.
9. Haduch, A., and Daniel, W.A. (2018). The engagement of brain cytochrome P450 in the metabolism of endogenous neuroactive substrates: a possible role in mental disorders. Drug Metab. Rev. *50*, 415–429. https://doi.org/10.1080/03602532.2018.1554674.
10. Pikuleva, I.A., and Cartier, N. (2021). Cholesterol Hydroxylating Cytochrome P450 46A1: From Mechanisms of Action to Clinical Applications. Front. Aging Neurosci. *13*, 696778. https://doi.org/10.3389/fnagi.2021.696778.
11. Pikuleva, I.A. (2023). Challenges and Opportunities in P450 Research on the Eye. Drug Metab. Dispos. *51*, 1295–1307. https://doi.org/10.1124/dmd.122.001072.
12. Omarova, S., Charvet, C.D., Reem, R.E., Mast, N., Zheng, W., Huang, S., Peachey, N.S., and Pikuleva, I.A. (2012). Abnormal vascularization in mouse retina with dysregulated retinal cholesterol homeostasis. J. Clin. Investig. *122*, 3012–3023. https://doi.org/10.1172/JCI63816.
13. Saadane, A., Mast, N., Charvet, C.D., Omarova, S., Zheng, W., Huang, S.S., Kern, T.S., Peachey, N.S., and Pikuleva, I.A. (2014). Retinal and Nonocular Abnormalities in Cyp27a1Cyp46a1 Mice with Dysfunctional Metabolism of Cholesterol. Am. J. Pathol. *184*, 2403–2419. https://doi.org/10.1016/j.ajpath.2014.05.024.
14. Saadane, A., Mast, N., Dao, T., Ahmad, B., and Pikuleva, I.A. (2016). Retinal Hypercholesterolemia Triggers Cholesterol Accumulation and Esterification in Photoreceptor Cells. J. Biol. Chem. *291*, 20427–20439. https://doi.org/10.1074/jbc.M116.744656.
15. Saadane, A., Mast, N., Trichonas, G., Chakraborty, D., Hammer, S., Busik, J.V., Grant, M.B., and Pikuleva, I.A. (2019). Retinal Vascular Abnormalities and Microglia Activation in Mice with Deficiency in Cytochrome P450 46A1-Mediated Cholesterol Removal. Am. J. Pathol. *189*, 405–425. https://doi.org/10.1016/j.ajpath.2018.10.013.
16. El-Darzi, N., Mast, N., Li, Y., Dailey, B., Kang, M., Rhee, D.J., and Pikuleva, I.A. (2023). The normalizing effects of the CYP46A1 activator efavirenz on retinal sterol levels and risk factors for glaucoma in Apoj−/− mice. Cell. Mol. Life Sci. *80*, 194. https://doi.org/10.1007/s00018-023-04848-y.
17. Fourgeux, C., Bron, A., Acar, N., Creuzot-Garcher, C., and Bretillon, L. (2011). 24S-hydroxycholesterol and cholesterol-24S-hydroxylase (CYP46A1) in the retina: from cholesterol homeostasis to pathophysiology of glaucoma. Chem. Phys. Lipids *164*, 496–499. https://doi.org/10.1016/j.chemphyslip.2011.04.006.
18. Fourgeux, C., Martine, L., Pasquis, B., Maire, M., Acar, N., Creuzot-Garcher, C., Bron, A., and Bretillon, L. (2012). Steady-state levels of retinal 24S-hydroxycholesterol are maintained by glial cells intervention after elevation of intraocular pressure in the rat. Acta Ophthalmol. *90*, e560–e567. https://doi.org/10.1111/j.1755-3768.2012.02490.x.
19. Léger-Charnay, E., Gambert, S., Martine, L., Dubus, E., Maire, M.A., Buteau, B., Morala, T., Gigot, V., Bron, A.M., Bretillon, L., and Masson, E.A.Y. (2022). Retinal cholesterol metabolism is perturbated in response

to experimental glaucoma in the rat. PLoS One *17*, e0264787. https://doi.org/10.1371/journal.pone.0264787.

20. Fourgeux, C., Martine, L., Björkhem, I., Diczfalusy, U., Joffre, C., Acar, N., Creuzot-Garcher, C., Bron, A., and Bretillon, L. (2009). Primary Open-Angle Glaucoma: Association with Cholesterol 24S-Hydroxylase (CYP46A1) Gene Polymorphism and Plasma 24-Hydroxycholesterol Levels. Investig. Ophthalmol. Vis. Sci. *50*, 5712. https://doi.org/10.1167/iovs.09-3655.
21. Bretillon, L., Diczfalusy, U., Björkhem, I., Maire, M.A., Martine, L., Joffre, C., Acar, N., Bron, A., and Creuzot-Garcher, C. (2007). Cholesterol-24S-hydroxylase (CYP46A1) Is Specifically Expressed in Neurons of the Neural Retina. Curr. Eye Res. *32*, 361–366. https://doi.org/10.1080/02713680701231857.
22. Capozzi, M.E., McCollum, G.W., and Penn, J.S. (2014). The Role of Cytochrome P450 Epoxygenases in Retinal Angiogenesis. Investig. Ophthalmol. Vis. Sci. *55*, 4253–4260. https://doi.org/10.1167/iovs.14-14216.
23. Song, Y.S., Zaitoun, I.S., Wang, S., Darjatmoko, S.R., Sorenson, C.M., and Sheibani, N. (2023). Cytochrome P450 1B1 Expression Regulates Intracellular Iron Levels and Oxidative Stress in the Retinal Endothelium. Int. J. Mol. Sci. *24*, 2420. https://doi.org/10.3390/ijms24032420.
24. Charlton-Perkins, M., and Cook, T.A. (2010). Building a Fly Eye. Curr. Top. Dev. Biol. *93*, 129–173. https://doi.org/10.1016/B978-0-12-385044-7.00005-9.
25. Kumar, J.P. (2012). Building an ommatidium one cell at a time: Ommatidial Assembly in Drosophila. Dev. Dyn. *241*, 136–149. https://doi.org/10.1002/dvdy.23707.
26. Chung, H., Sztal, T., Pasricha, S., Sridhar, M., Batterham, P., and Daborn, P.J. (2012). Characterization of Drosophila melanogaster cytochrome P450 genes. Proc. Natl. Acad. Sci. USA *106*, 5731–5736. https://doi.org/10.1073/pnas.0812141106.
27. Giraudo, M., Unnithan, G.C., Le Goff, G., and Feyereisen, R. (2010). Regulation of cytochrome P450 expression in Drosophila: Genomic insights. Pestic. Biochem. Physiol. *97*, 115–122. https://doi.org/10.1016/j.pestbp.2009.06.009.
28. Good, R.T., Gramzow, L., Battlay, P., Sztal, T., Batterham, P., and Robin, C. (2014). The Molecular Evolution of Cytochrome P450 Genes within and between Drosophila Species. Genome Biol. Evol. *6*, 1118–1134. https://doi.org/10.1093/gbe/evu083.
29. Tijet, N., Helvig, C., and Feyereisen, R. (2001). The cytochrome P450 gene superfamily in Drosophila melanogaster : Annotation, intron-exon organization and phylogeny. Gene *262*, 189–198. https://doi.org/10.1016/S0378-1119(00)00533-3.
30. Phillips, S.E., Woodruff, E.A., Liang, P., Patten, M., and Broadie, K. (2008). Neuronal Loss of Drosophila NPC1a Causes Cholesterol Aggregation and Age-Progressive Neurodegeneration. J. Neurosci. *28*, 6569–6582. https://doi.org/10.1523/JNEUROSCI.5529-07.2008.
31. Van Den Brink, D.M., Cubizolle, A., Chatelain, G., Davoust, N., Girard, V., Johansen, S., Napoletano, F., Dourlen, P., Guillou, L., Angebault-Prouteau, C., et al. (2018). Physiological and pathological roles of FATP-mediated lipid droplets in Drosophila and mice retina. PLoS Genet. *14*, e1007627. https://doi.org/10.1371/journal.pgen.1007627.
32. Ravindranath, V., and Strobel, H.W. (2013). Cytochrome P450-mediated metabolism in brain: functional roles and their implications. Expert Opin. Drug Metab. Toxicol. *9*, 551–558. https://doi.org/10.1517/17425255.2013.759208.
33. Oka, M., Nakajima, S., Suzuki, E., Yamamoto, S., and Ando, K. (2025). Glucose uptake in pigment glia suppresses Tau-induced inflammation and photoreceptor degeneration. Dis. Model. Mech. *18*, dmm052057. https://doi.org/10.1242/dmm.052057.
34. McMullen, E., Hertenstein, H., Strassburger, K., Deharde, L., Brankatschk, M., and Schirmeier, S. (2023). Glycolytically impaired Drosophila glial cells fuel neural metabolism via β-oxidation. Nat. Commun. *14*, 2996. https://doi.org/10.1038/s41467-023-38813-x.
35. Hurley, J.B., Lindsay, K.J., and Du, J. (2015). Glucose, lactate, and shuttling of metabolites in vertebrate retinas. J. Neurosci. Res. *93*, 1079–1092. https://doi.org/10.1002/jnr.23583.
36. Moulton, M.J., Barish, S., Ralhan, I., Chang, J., Goodman, L.D., Harland, J.G., Marcogliese, P.C., Johansson, J.O., Ioannou, M.S., and Bellen, H.J. (2021). Neuronal ROS-induced glial lipid droplet formation is altered by loss of Alzheimer's disease–associated genes. Proc. Natl. Acad. Sci. USA *118*, e2112095118. https://doi.org/10.1073/pnas.2112095118.
37. Serrano, J., Martine, L., Grosjean, Y., Acar, N., Alves, G., and Masson, E.A.Y. (2024). The importance of choosing the appropriate cholesterol quantification method: enzymatic assay versus gas chromatography. J. Lipid Res. *65*, 100561. https://doi.org/10.1016/j.jlr.2024.100561.
38. Brooks, S.W., Dykes, A.C., and Schreurs, B.G. (2017). A High-Cholesterol Diet Increases 27-Hydroxycholesterol and Modifies Estrogen Receptor Expression and Neurodegeneration in Rabbit Hippocampus. J. Alzheimers Dis. *56*, 185–196. https://doi.org/10.3233/JAD-160725.
39. Thirumangalakudi, L., Prakasam, A., Zhang, R., Bimonte-Nelson, H., Sambamurti, K., Kindy, M.S., and Bhat, N.R. (2008). High cholesterol-induced neuroinflammation and amyloid precursor protein processing correlate with loss of working memory in mice. J. Neurochem. *106*, 475–485. https://doi.org/10.1111/j.1471-4159.2008.05415.x.
40. Liu, Q., An, Y., Ma, W., Feng, L., Wang, C., Lu, Y., and Xiao, R. (2017). High-cholesterol diet results in elevated amyloid-β and oxysterols in rats. Mol. Med. Rep. *17*, 1235–1240. https://doi.org/10.3892/mmr.2017.8003.
41. Zanco, B., Mirth, C.K., Sgrò, C.M., and Piper, M.D. (2021). A dietary sterol trade-off determines lifespan responses to dietary restriction in Drosophila melanogaster females. eLife *10*, e62335. https://doi.org/10.7554/eLife.62335.
42. Danielson, P.B., and Fogleman, J.C. (1997). Isolation and sequence analysis of cytochrome P450 12B1: the first mitochondrial insect P450 with homology to lα,25 dihydroxy-D3 24-hydroxylase. Insect Biochem. Mol. Biol. *27*, 595–604. https://doi.org/10.1016/S0965-1748(97)00035-0.
43. Prosser, D.E., and Jones, G. (2004). Enzymes involved in the activation and inactivation of vitamin D. Trends Biochem. Sci. *29*, 664–673. https://doi.org/10.1016/j.tibs.2004.10.005.
44. Omura, T. (2006). Mitochondrial P450s. Chem. Biol. Interact. *163*, 86–93. https://doi.org/10.1016/j.cbi.2006.06.008.
45. Veith, A., and Moorthy, B. (2018). Role of cytochrome P450S in the generation and metabolism of reactive oxygen species. Curr. Opin Toxicol. *7*, 44–51. https://doi.org/10.1016/j.cotox.2017.10.003.
46. Zangar, R.C., Davydov, D.R., and Verma, S. (2004). Mechanisms that regulate production of reactive oxygen species by cytochrome P450. Toxicol. Appl. Pharmacol. *199*, 316–331. https://doi.org/10.1016/j.taap.2004.01.018.
47. Catalani, E., Brunetti, K., Del Quondam, S., and Cervia, D. (2023). Targeting Mitochondrial Dysfunction and Oxidative Stress to Prevent the Neurodegeneration of Retinal Ganglion Cells. Antioxidants *12*, 2011. https://doi.org/10.3390/antiox12112011.
48. Brown, E.E., DeWeerd, A.J., Ildefonso, C.J., Lewin, A.S., and Ash, J.D. (2019). Mitochondrial oxidative stress in the retinal pigment epithelium (RPE) led to metabolic dysfunction in both the RPE and retinal photoreceptors. Redox Biol. *24*, 101201. https://doi.org/10.1016/j.redox.2019.101201.
49. Gruenewald, C., Botella, J.A., Bayersdorfer, F., Navarro, J.A., and Schneuwly, S. (2009). Hyperoxia-induced neurodegeneration as a tool to identify neuroprotective genes in Drosophila melanogaster. Free Radic. Biol. Med. *46*, 1668–1676. https://doi.org/10.1016/j.freeradbiomed.2009.03.025.
50. Jaiswal, M., Haelterman, N.A., Sandoval, H., Xiong, B., Donti, T., Kalsotra, A., Yamamoto, S., Cooper, T.A., Graham, B.H., and Bellen, H.J. (2015). Impaired Mitochondrial Energy Production Causes Light-Induced Photoreceptor Degeneration Independent of Oxidative Stress. PLoS Biol. *13*, e1002197. https://doi.org/10.1371/journal.pbio.1002197.

51. Eells, J.T. (2019). Mitochondrial Dysfunction in the Aging Retina. Biology *8*, 31. https://doi.org/10.3390/biology8020031.

52. Zhou, B., Fang, L., Dong, Y., Yang, J., Chen, X., Zhang, N., Zhu, Y., and Huang, T. (2021). Mitochondrial quality control protects photoreceptors against oxidative stress in the H2O2-induced models of retinal degeneration diseases. Cell Death Dis. *12*, 413. https://doi.org/10.1038/s41419-021-03660-5.

53. Robinow, S., and White, K. (1988). The locus *elav* of *Drosophila melanogaster* is expressed in neurons at all developmental stages. Dev. Biol. *126*, 294–303. https://doi.org/10.1016/0012-1606(88)90139-X.

54. Charlton-Perkins, M.A., Sendler, E.D., Buschbeck, E.K., and Cook, T.A. (2017). Multifunctional glial support by Semper cells in the Drosophila retina. PLoS Genet. *13*, e1006782. https://doi.org/10.1371/journal.pgen.1006782.

55. Jung, W.H., Liu, C.C., Yu, Y.L., Chang, Y., Lien, W., Chao, H., Huang, S., Kuo, C., Ho, H., and Chan, C. (2017). Lipophagy prevents activity-dependent neurodegeneration due to dihydroceramide accumulation in vivo. EMBO Rep. *18*, 1150–1165. https://doi.org/10.15252/embr.201643480.

56. Awasaki, T., Lai, S.L., Ito, K., and Lee, T. (2008). Organization and Postembryonic Development of Glial Cells in the Adult Central Brain of Drosophila. J. Neurosci. *28*, 13742–13753. https://doi.org/10.1523/JNEUROSCI.4844-08.2008.

57. Rezával, C., Pavlou, H.J., Dornan, A.J., Chan, Y.B., Kravitz, E.A., and Goodwin, S.F. (2012). Neural Circuitry Underlying Drosophila Female Postmating Behavioral Responses. Curr. Biol. *22*, 1155–1165. https://doi.org/10.1016/j.cub.2012.04.062.

58. Folch, J., Lees, M., and Stanley, G.H.S. (1957). A simple method for the isolation and purification of total lipides from animal tissues. J. Biol. Chem. *226*, 497–509. https://doi.org/10.1016/s0021-9258(18)64849-5.

59. Dourlen, P., Levet, C., Mejat, A., Gambis, A., and Mollereau, B. (2013). The Tomato/GFP-FLP/FRT Method for Live Imaging of Mosaic Adult Drosophila Photoreceptor Cells. JoVE J. *2013*, e50610. https://doi.org/10.3791/50610.

60. Schindelin, J., Arganda-Carreras, I., Frise, E., Kaynig, V., Longair, M., Pietzsch, T., Preibisch, S., Rueden, C., Saalfeld, S., Schmid, B., et al. (2012). Fiji: an open-source platform for biological-image analysis. Nat. Methods *9*, 676–682. https://doi.org/10.1038/nmeth.2019.

61. Hsiao, H.Y., Johnston, R.J., Jukam, D., Vasiliauskas, D., Desplan, C., and Rister, J. (2012). Dissection and immunohistochemistry of larval, pupal and adult Drosophila retinas. J. Vis. Exp. *2012*, 4347. https://doi.org/10.3791/4347.

STAR★METHODS

KEY RESOURCES TABLE

REAGENT or RESOURCE	SOURCE	IDENTIFIER
Chemicals, peptides, and recombinant proteins		
Cholesterol	Sigma-Aldrich, St Quentin-Fallavier, France	Cat#C8667
TRIzol	Invitrogen™, Waltham, MA, USA	Cat#15596026
RNase-free DNase I	Thermo scientific, MA, USA	Cat#EN0521
FastSYBRTM Green Master Mix	Thermo scientific, MA, USA	Cat#4385612
Paraformaldehyde 16% aqueous solution EM grade	Electron Microscopy Sciences	Cat#15710
Normal Growth Serum	Merck, Saint-Quentin-Fallavier, France	Cat#G9023,
Phalloidin-iFluor 488 reagent	abcam, Cambridge, UK	Cat#ab176753
Phalloidin-iFluor 647 reagent	abcam, Cambridge, UK	Cat#ab176759
Alexa Fluor® 647 Phalloidin	Ozyme, Saint-Cyr-l'Ecole, France	Cat#8940S
HCS LipidTOX™ Red Neutral Lipid Stain	Thermo Scientific, MA, USA	Cat#H34476
Nile Red	Merck, Saint-Quentin-Fallavier, France	Cat#72485
VECTASHIELD® mounting medium	Vector Laboratories, Peterborough, UK	Cat#H-1000
Toluidine blue	Fluka	Cat#89640
Critical commercial assays		
iScript cDNA synthesis kit	BioRad, Hercules, CA, USA	Cat#1708840
Bicinchoninic acid (BCA) protein assay kit	Pierce Biotechnology, Thermo Scientific, MA, USA	Cat#10678484
Experimental models: Organisms/strains		
D. melanogaster: Canton S	Bloomington Drosophila Stock Center	BDSC Cat#64349
D. melanogaster: GMR-Gal4	Bloomington Drosophila Stock Center	BDSC Cat#1104
D. melanogaster: GMR-hid	Bloomington Drosophila Stock Center	BDSC Cat#5771
D. melanogaster: UASnlsGFP	Bloomington Drosophila Stock Center	BDSC Cat#4776
D. melanogaster: tubulin-Gal80ts	Bloomington Drosophila Stock Center	BDSC Cat#7017
D. melanogaster: repo-Gal80	Gift from Dr. Yuh Nung Jan[56]	N/A
D. melanogaster: elav-Gal80	gift from Dr. Carolina Rezával[57]	N/A
D. melanogaster: UAS-Dmcyp12c1dsRNAGD	Vienna Drosophila Resource Center	VDRC Cat# GD34807
D. melanogaster: UAS-Dmcyp12a5dsRNAGD	Vienna Drosophila Resource Center	VDRC Cat# GD26796
D. melanogaster: Dmcyp49a1dsRNAKK	Vienna Drosophila Resource Center	VDRC Cat# KK101530
Oligonucleotides		
Please refer Table S1	N/A	N/A
Software and algorithms		
NIST bank	The NIST/EPA/NIH Mass Spectral Library Version 2.0f, build Oct 8 2008	N/A
ImageJ Software, USA	National Institute of Health	https://imagej.nih.gov/ij/
Leica LAS AF software	Leica Microsystems	https://www.leica-microsystems.com/products/microscope-software/
Excel	Microsoft	https://products.office.com/en-gb/exce
GraphPad Prism	GraphPad	https://www.graphpad.com/
Other		
Tissue Lyser	Qiagen, Venlo, The Netherlands	N/A

(*Continued on next page*)

Continued

REAGENT or RESOURCE	SOURCE	IDENTIFIER
Leica TCS SP8 microscope	Leica Microsystems	https://www.leica-microsystems.com/
Leica M165FC microscope	Leica Microsystems	https://www.leica-microsystems.com/
Gas chromatography coupled to a mass spectrometer	Agilent; Santa Clara, CA	#5973N

EXPERIMENTAL MODEL AND STUDY PARTICIPANT DETAILS

Fly stocks and rearing conditions

Drosophila melanogaster males were exclusively used in all experiments and were maintained under a 12-hour light/dark cycle. Flies were reared at 25°C, except for experiments involving thermosensitive transgenes. In those cases, flies were raised at 18°C to prevent dsRNA expression during development and were transferred to 28°C to induce dsRNA expression post-emergence. From their emergence, the flies were raised on two distinct diets, each comprised of brewer's yeast E50 (0.065 g / mL, MP Biomedicals, Illkirch-Graffenstaden, France), corn flour (0.065 g / ml, Eurogerm, Saint-Apollinaire, France), agar (0.009 g / mL, Groupe MERIDIS, Montpellier, France), tegosept (3.1%, Genesee Scientific, San Diego, CA), and water. Cholesterol (#C8667 Sigma-Aldrich, St Quentin-Fallavier, France, 0.1 g / L) was added to the cholesterol-supplemented diet, while the ethanol vehicle was added to the control diet.

METHOD DETAILS

Selection of *Drosophila* Dmcyp gene

The Hugo Gene Nomenclature Committee (HGNC) website enabled us to predict homologies between human CYP27A1 protein and proteins from other species, such as *Drosophila melanogaster* (Dm). Only DmCYP with unidentified functions were selected. Then, we used the DRSC integrative ortholog predictive tool (DIOP) in the Harvard medical school website to perform a Basic Local Alignment Search Tool (BLAST) between human CYP27A1 protein and its predicted Drosophila homolog proteins. From these protein alignments, the percentage of amino acid similarity and identity between Drosophila protein and human CYP27A1 proteins were obtained.

Gene expression analysis by real time qPCR

RNA from 6 biological replicates of 20 7-day-old Drosophila heads per genotype was isolated. Briefly, heads were dissected on ice and placed immediately in TRIzol (Invitrogen™, Waltham, MA, USA) and then frozen at -80°C until use. Samples were lysed using tungsten microbeads in a Tissue Lyser (Qiagen, Venlo, The Netherlands, 1 min 30 s at 30 Hz speed). After RNA isolation with chloroform/isopropanol extraction, samples were treated with RNase-free DNase I (1 U / mL, Thermo scientific, MA, USA) to eliminate contamination with genomic DNA. Then, cDNA was synthesized using iScript cDNA synthesis kit (BioRad, Hercules, CA, USA). Real-time PCR was performed with FastSYBRTM Green Master Mix (#4385612, Applied Biosystem, ThermoFisher Scientific, Waltham, MA, USA), according to a standardized procedure (Applied Biosystems™ and Roche). Relative quantification (RQ) values were calculated by using the $2-\Delta\Delta Ct$ method, with Rp49 serving as the housekeeping gene. The sequence of qPCR primers used is presented in Table S1.

Cholesterol quantification by gas chromatography coupled to mass spectrometry (GC-MS)

Fly retinas were dissected in PBS on ice. When flies were raised on standard food, three biological replicates were performed, each replicate consisting of 150 retinas collected from 75 flies. When flies were reared on cholesterol-supplemented food, six biological replicates were used, each consisting of 30 retinas. 7-10-day-old and 30-35-day-old Drosophila were used to represent the young and aged group, respectively. Then, retinas were snap frozen in liquid nitrogen and stored at -80°C. Before lipid extraction, samples were homogenized in 1 mL distilled water with tungsten microbeads using a Tissue Lyser (Qiagen, Venlo, The Netherlands, 1 min 30 s at 30 Hz speed). A small aliquot of 30 μL of the homogenate was collected for protein quantification. Lipids were extracted from the remaining homogenate according to Folch's procedure.[58] Briefly, the homogenate was mixed with 5 mL of chloroform/methanol mixture (2:1, v/v). After centrifugation (1620 g, 3 min, room temperature (RT)), the lower organic phase containing lipids was isolated. Total lipids were then dried under nitrogen and submitted to alkaline hydrolysis to extract sterols, which cannot be saponified. Cholesterol was analyzed from the total non-saponified material, after trimethylsilyl ether derivation using BSTFA/TMCS (99:1, v/v) at 60°C for 30 min and addition of cholesterol-d7. Cholesterol was identified and quantified using gas chromatography coupled to a mass spectrometer (5973N, Agilent; Santa Clara, CA) equipped with a DB-5MS column of 30 m (length) x 0.25 mm (internal diameter) x 0.25 μm (internal coating) (Agilent, Santa Clara, CA). Samples were injected using spitless mode at 290°C and separated under a temperature gradient as follows: 1 min 60°C, 20°C/min up to 290°C. Cholesterol was identified in scan mode according to its retention time and its specific spectra compared to the NIST bank (The NIST/EPA/NIH Mass Spectral Library Version 2.0f, build Oct 8 2008). Finally, cholesterol was quantified using a calibration curve and the cholesterol-d7 internal standard.

Quantitative determination of protein contents

Aliquots of tissue homogenates were lysed with 5X Ripa buffer, followed by a 30 min incubation on ice. The lysates were then centrifuged at 15300 g for 10 min at 4°C. Total protein content in the supernatants was quantified using the Bicinchoninic acid (BCA) protein assay kit, following the manufacturer's instructions (Pierce Biotechnology, Thermo Scientific, MA, USA), with bovine serum albumin as a standard (Sigma-Aldrich, USA).

Whole eye imaging

For imaging adult eyes, the 3-day-old flies were immobilized following the protocol of Dourlen et al.[59] Briefly, agarose (1.5% in 100 mL of water) was dissolved and heated in a microwave, then transferred into a 35 x 10 mm petri dish. Before agarose solidification, Drosophila were anesthetized with CO2 for 1 min and placed on the warm agarose. Using fine forceps and a binocular magnifying glass, the flies were quickly oriented, with one wing pressed into the agarose. These flies were then imaged with Leica M165FC microscope using LasX software. Eye images were captured from 10 different flies. The eye area was defined using the FIJI software.[60]

Immunohistochemistry

Retinas from 7–10- or 30–35-day-old flies were used using either cryosections or whole-retina dissection.

Drosophila head cryosection

For section, adult flies were anesthetized on ice and the proboscis was removed. Then, flies were fully submerged in 4% paraformaldehyde (PFA) in phosphate-buffered saline (PBS) for 30 min at RT, then rinsed three times in PBS and one time in a sucrose solution (25% in dH2O). Samples were cryoprotected by incubation in the sucrose solution overnight at 4°C. Flies were decapitated and the heads were embedded in optimal cutting temperature (OCT) compound and rapidly frozen. Cryosections (14 μm thick) were cut at −20 °C using a cryostat and collected on Superfrost Plus glass slides. Sections were air-dried and stored at −20 °C until further processing for staining. For the staining, cryosections were air-dried for 15 min at RT. Sections were then washed in PBS containing 0.1% Triton X-100 (PBST) and incubated in a blocking solution (PBS-T 0,3%, NGS (Normal Growth Serum) 5% (#G9023, Merck, Saint-Quentin-Fallavier, France) for 20 min at RT in order to prevent nonspecific binding. To visualize F-actin, which is abundant in photoreceptor, samples were then incubated overnight at 4°C with either phalloidin-iFluor 488 reagent (ab176753, 1:1000, abcam, Cambridge, UK) or phalloidin-iFluor 647 reagent (ab176759, 1:1000, abcam, Cambridge, UK) in PBS. Neutral lipids, which are enriched in lipid droplets, were labeled using HCS LipidTOX™ Red Neutral Lipid Stain (#H34476, 1:1000, Thermo Scientific, MA, USA) in PBS overnight at 4°C, or alternatively with Nile Red (#72485, 1:1000, Merck, Saint-Quentin-Fallavier, France) in PBS, 20 min at RT the following day. Sample nuclei were stained with DAPI (1:1000) during 10min at RT. Sections were subsequently washed 3 times for 10 min each in PBS at RT. Finally, sections were mounted using VECTASHIELD® mounting medium (H-1000, Vector Laboratories, Peterborough, UK) before visualization with a Leica TCS SP8 confocal microscope.

Whole-mount retina

Fly retinas were dissected in PBS on ice, keeping the Lamina, and fixed in 4% PFA for 30 min at RT. After washes (6 x 10 min with PBST 0,3% and 1 x 10 min with PBST 1%), aspecific sites were blocked with 10% NGS during 30 min at RT. During this incubation time, Lamina was removed from each retina. Finally, retinas were incubated with phalloidin coupled with Alexa fluor ® 647 (#8940S, Ozyme, Saint-Cyr-l'Ecole, France) in PBS (1/20) for 20 minutes at RT before washing with PBS (3 x 5 min). Adult retinas were mounted according to Hsiao's protocol.[61] Briefly, 5μL of 50% glycerol were put on both ends of a glass side, before covering them with 22x22-1 cover slips (0.13 to 0.17 mm thick). Finally, VECTASHIELD® mounting medium (H-1000, Vector Laboratories, Peterborough, UK) was used before visualization with a Leica TCS SP8 confocal microscope.

Toluidine blue staining

About 3-4 heads from 30–35-day-old flies per genotype (controls and *Dmcyp12c1* downregulated) were used. Heads were cut in two before being fixed for 45 min in 2,5% glutaraldehyde in Sorensen phosphate buffer (0.1 M, pH 7.2) at 4°C. Half fly heads were washed 6 times (1 x 30 min, 5 x 5 min) with Sorensen phosphate Buffer (0.1 M pH 7.2), followed by a post fixation at 4°C in 2% OsO4 (#19150, EMS) for 1h30 and additional washes (4 x 5min) in Sorensen phosphate buffer. Then samples were dehydrated in a standard EtOH series (30%, 50%, 70%, 95%, 100%) and then in acetone. Progressively, acetone was replaced by the Epon resin (Embed-812 #14900, EMS mixed with NMA #19000, EMS and DDSA #13710, EMS) (overnight at ¾th of Epon resin). Finally, samples were infiltrated during 2h up to overnight into Epon. Heads were positioned so that the retina was in contact with the blade. Polymerization was carried out by adding a preform filled with Epon and 3% BDMA (#11400-25, EMS), 1h at RT and then, until 3 days at 65°C. To reach the region of interest, twenty-five semithin serial sections (1.0 μm each) were removed. Once the region of interest was reached, 40 μm-tissue sections were collected on glass slides, stained with 0.5% toluidine blue (#89640, Fluka) on a hot plate at 80°C for 30 s, and rinsed with water. Sections were dried on the hot plate before being mounted with Pertex (#LEIC811, Leica). The experiments were performed at the ImaFlow facility part of the US58 BioSanD.

QUANTIFICATION AND STATISTICAL ANALYSIS

Retinal thickness measurement

Retinal thickness was assessed on 14-μm-thick Drosophila head cryosections stained with phalloidin to visualize the F-actin-rich photoreceptors. Retinal thickness was measured using FIJI/ImageJ by measuring the distance between the outer and inner boundaries of the retinal layer. Three measurements were performed per retina at defined positions, and the same regions of interest (ROIs) were recorded and used consistently across samples. Measurements were performed on young (7–12-day-old) and aged (30–35-day-old) flies, and values were expressed relative to the corresponding control genotype.

Statistical analysis

The Shapiro-Wilk test was used to test normality. Data were analyzed using GraphPad Prism9 software (GraphPad Software, San Diego, USA). For comparison of multiple groups, statistical significance was determined using ordinary one-way ANOVA with correction for multiple comparisons with Tukey test. When data distributions had unequal variance, P for two-group comparisons was computed using an unpaired t-test. Outlier values were identified and excluded with the ROUT method (Q = 1%). Data are represented as mean ± SEM. Statistical significance is indicated as *: $p < 0.05$, **: $p < 0.01$, ***: $p < 0.001$ or ****: $p < 0.0001$.